D2D Communication for Enabling Internet-of-Things: Outage Probability Analysis

Basem M. ElHalawany, *Member, IEEE*, and Rukhsana Ruby *Member, IEEE*, and Kaishun Wu *Member, IEEE*

***Abstract*—This work considers an analytical approach to evaluate the outage behavior of the device-to-device (D2D) communication, that is underlaid with cellular networks, as an enabling technology for Internet-of-Things (IoTs). In such an architecture, a group of IoT devices (IoTDs) communicate with an IoT gateway (GW) by reusing the resources of cellular users (CUEs) to enhance the spectral efficiency of the fifth-generation (5G) networks. Two interference management schemes are widely used in the literature for the sharing of D2D spectrum, namely the fixed-power margin (FPM) and the cooperative pairing (CooP) schemes. We investigate and compare the performance of the two schemes from the perspective of outage probability (OP). While satisfying the minimal performance of the system, the OP of an arbitrary pair (i.e., one IoTD and one CUE) under both the interference management schemes are derived in closed form in terms of hyper-geometric functions via the Mellin transform technique. Moreover, for the CooP scheme, an iterative alternating Dinkelbach (IAD) algorithm is proposed as an outage-optimal power allocation scheme. Analytical and simulation results reveal that the CooP scheme is the outage-optimum for the high SNR regime while the FPM scheme is the optimal one for the low SNR regime. Simulation results also show that the suitable power margin of the FPM scheme lies in between 2 and 3 dB. Under these two interference management schemes, the accuracy of the analytical results is verified through numerical simulation and it turns out that they are well matched.**

***Index Terms*—Internet-of-Things; Device-to-Device Communication; Interference Management; Mellin Transform; Outage Probability**

I. Introduction

In the recent years, researchers have been investigating potential solutions for supporting the deployment scenarios for Internet-of-Things (IoTs) applications. With the development of IoT, the fifth-generation (5G) mobile communication networks are expected to deal with a drastic increase in mobile traffic [1], with an expectation of 50 billion IoT connections by 2020. With this huge demand of resources to support such massive connectivity, the current orthogonal multiple access (OMA) technologies, such as orthogonal frequency-division multiple access (OFDMA), time-division multiple access (TDMA) and code-division multiple access (CDMA), are not sufficient [2]. One of the main reasons for this shortage and expected congestion in the OMA techniques is the low spectral efficiency especially when a subcarrier is allocated to a user with poor channel conditions [3]. In other words, the OMA techniques do not allow to serve multiple users on the same resource element (i.e., frequency, time and code) simultaneously.

Two technologies are introduced recently to partially solve the congestion problem that is expected to be faced by future 5G networks, namely device-to-device (D2D) communication and non-orthogonal multiple access (NOMA). The first one is based on allowing some sort of controllable interference among multiple nodes, also known as reuse partners, to share the same resource blocks (RBs) [4]. Each reuse partner considers interference from other nodes as noise. The second technology is based on the concept of adopting the superposition coding technique at the transmitter side and the successive interference cancellation (SIC) technique at the receiver side. Through this concept, the signals of strong users can be recovered easily assuming interference signals resulting from other weak users as noise. As a result, the signals of strong users can be decoded and removed successfully one-by-one in an iterative manner from the received superposition-coded signal [3].

Recently, the interplay between D2D communication and IoT applications is drawing tremendous attention [5]–[7]. Different protocols have been proposed to investigate the coexistence of these technologies by exploiting the proximity in D2D communication for reliable transmission. In [6], the authors proposed a two-phase downlink transmission protocol for achieving ultra-reliable and low latency communications (URLLC) between the base station (BS) and a group of clustered IoT devices (IoTDs) in an automated factory system. D2D communication is used as a means for delivering a reliable proximity transmission mechanism from the cluster-head to IoTDs in the second phase. The authors in [8] adopted the D2D communication technique as a route extension model of narrowband IoT (NB-IoT) systems, which was introduced by the Third Generation Partnership Project (3GPP) to provide low-power and wide-area coverage for IoTs, and thus enables two-hop routes between NB-IoT nodes and the serving BS via a set of D2D relays. On the other hand, the work in [7] investigated the impact of intelligent D2D communication in the IoT environment considering that devices are the main users in the IoT ecosystem and D2D communication as an intrinsic part of the IoT applications. The authors analyzed the state-of-the-art communication mechanisms in licensed

This paragraph of the first footnote will contain the date on which you submitted your brief for review.

Basem M. ElHalawany is with Smart Sensing and Mobile Computing laboratory, School of Computer Science and Software Engineering, Shenzhen University, Shenzhen 518060, China. Basem is also with the Faculty of Engineering at Shoubra, Benha University, Egypt (e-mail: basem.mamdoh@feng.bu.edu.eg, basem.mamdoh@szu.edu.cn).

Rukhsana Ruby and Kaishun Wu are with Smart Sensing and Mobile Computing laboratory, School of Computer Science and Software Engineering, Shenzhen University, Shenzhen 518060, China (e-mail: ruby@szu.edu.cn, wu@szu.edu.cn).

and unlicensed spectral bands and routing techniques that can support intelligent D2D communications.

In this work, we consider the D2D communication as a low-complexity spectrum sharing technique that allows a CUE and an IoTD to share the same spectrum band in order to facilitate a cluster-based IoT deployment scenario at which a group of IoTDs are uniformly deployed in the vicinity of a cluster head device that works as a gateway for the entire cluster [5]. Each IoTD within the cluster reuses the RBs of one of the cellular users (CUEs) if both partners can achieve their pre-defined quality-of-service (QoS) requirements. In other words, a CUE is considered as a candidate reuse partner if the corresponding IoTD can access its RB without introducing harmful interference. Therefore, we find it required to study the outage probability (OP) of underlying cluster-based D2D devices in cellular networks, which is a topic that is not fully investigated up to the knowledge of the authors.

Notice that the aforementioned scenario is different from the D2D ad-hoc scenarios at which multiple D2D transceiver pairs communicate under cellular networks [9]–[11]. Most of the research work have considered ad-hoc scenario while there are few investigations that considered the cluster-based D2D scenario [5], which is naturally suitable for IoT deployment.

In order to investigate the OP of an arbitrary pair, we require to fix an interference management scheme to control the allowable mutual interference. To this end, we derive and compare the OP for two interference management schemes, namely the fixed power margin (FPM) [5], [9], [10] and the cooperative pairing (CooP) schemes [11], [12]. In the FPM scheme, a power margin in the signal-to-interference-plus-noise ratio (SINR) of a CUE is assumed to compensate the interference introduced by the D2D transmitters. In other words, a margin Υ is assumed in the SINR requirement for the BS, which corresponds to the allowable interference in the network. However, D2D reuse of the CUE channels should not cause their SINR to fall below the allowable margin (Υ). In contrast to the FPM scheme, there is no such protective power margin in the CooP scheme where both terminals in a pair cooperate to adjust their transmit power for satisfying the QoS requirements at both destinations. Exploring such cooperative model is proved to be efficient for throughput maximization in ad-hoc D2D networks [11]. However, we need to ask if such cooperative scheme is efficient from the perspective of OP in a cluster-based IoT network which will be revealed in this work.

In the context of this work, we summarize a survey report in Table I, which compares a group of works in terms of the adopted interference management scheme, deployment scenario and the derivation of OP or not. The authors in [5] investigated the reuse conditions of the interference-limited FPM scheme (i.e., power spectral density of noise N_o is negligible compared to the IoTD interference power) and they established a one-to-one matching model between CUEs and IoTDs for the purpose of throughput maximization in a cluster-based D2D deployment scenario. However, the OP is not derived or considered in this work. The authors in [9], [10] investigated the reuse conditions in the FPM scheme for an ad-hoc deployment scenario. The system OP is evaluated using simulation methods in [9] and derived based on geometric methods using numerical integration in [10] with no closed-form expression. In [12], the OP of D2D users in the CooP scheme under an ad-hoc D2D deployemnt scenario is investigated without considering the QoS requirements of the paired CUEs. The D2D OP in [12] is derived by exploiting the stochastic geometry and the Laplace transformation technique. Similar to [12], the work in [13] exploits the stochastic geometry to present an analytical framework for deriving the coverage probability (i.e., 1- outage probability) for an overlaid D2D network at which the network resources are orthogonally divided between D2D and cellular users with the location of devices modeled as a Poisson cluster process (PCP). In [11], the authors proposed a power allocation scheme for maximizing the system throughput under the ad-hoc CooP scheme without the derivation or consideration of OP.

TABLE I: A Survey on the OP Analysis

Reference	FPM or CooP	Clustered or Ad-hoc	Analytic or Simulation	OP Definition
[5]	FPM	Clustered	Not Investigated	-
[9]	FPM	Ad-hoc	Simulation	System OP
[10]	FPM	Ad-hoc	Numerical Integration (No closed-form expression)	System OP
[11]	CooP	Ad-hoc	Not Investigated	-
[12]	CooP	Ad-hoc	Analytic	D2D OP

Since the clustered D2D model is more suitable to the IoT deployment scenario, we consider such a system model in this work. While considering the QoS requirement of the CUE and IoTDs in such a system, we derive the closed-form expressions of the OP for an arbitrary CUE-IoTD pair under the FPM and CooP interference management schemes, which is to the best of our knowledge has not been fully investigated. The major contributions in this work are listed as follows.

- We propose a modified reuse condition for the FPM scheme based on the exact SINR analysis.
- We derive a closed-form expression of the OP for an arbitrary CUE-IoTD pair, under the interference-limited [1] FPM scheme in [5] and the proposed exact FPM scheme, for a cluster-based D2D scenario in terms of hyper-geometric MeijerG functions [17], [18] via the Mellin Transformation technique [19]–[21].
- We derive a closed-form expression of the OP for an arbitrary CUE-IoTD pair under the CooP scheme in a cluster-based D2D scenario. Moreover, we propose an outage-optimal power allocation technique for the CooP scheme using the iterative alternating Dinkelbach (IAD) algorithm.
- The accuracy of the analytical results under different interference management schemes is verified through extensive numerical simulation.

Note that the cluster-based D2D model and the proposed solution can also be applied to specific vehicular communication scenarios at which a Road Side Units (RSU) is employed

[1] In an interference-limited scheme, the noise power is considered as negligible compared to the interference power as in [14]–[16].

as the gateway to communicate with the vehicles in its vicinity to deliver data to/from other vehicles. In this case, gateway-enabled RSUs can provide different Internet services to the vehicles via cellular networks. Due to the scarcity of spectrum, D2D communications inside the vehicles are required to share the RBs with the legitimate CUEs.

The rest of the paper is organized as follows. In Section II, we describe the system model while illustrating the QoS requirements. Then, we introduce two interference management schemes under consideration in Section III. The OP for both schemes are derived in Section IV, and an outage-optimal CooP power allocation scheme is proposed in Section V. In Section VI, we verify the derived analytical results via simulation. Finally, the paper is concluded in Section VII which is followed by appendices.

Notations: The mathematical notations used in this work are as follows. $Pr\{A\}$ is the probability of event A, $f_X(.), F_X(.), M_X(s)$ are the probability density function (PDF), cumulative distribution function (CDF) and the Mellin transformation technique of the random variable X, respectively. $f_{XY}(X,Y)$ is the joint PDF for the two random variables X and Y. $\Gamma(.)$ is the Gamma function. $K_n(.)$ is the modified Bessel function of the second order. $G_{p\ q}^{m\ n}\left(\begin{smallmatrix}a_1,\ldots,a_p\\ b_1,\ldots,b_q\end{smallmatrix}\middle|z\right)$ is the hyper-geometric MeijerG function, $U(.)$ is the unit-step function. Finally, the $x \sim \mathcal{CN}(\mu,\sigma)$ means that x is a complex variable with the Gaussian distribution that has μ mean and σ variance.

II. Network Model

In this work, we focus on a single-cell uplink scenario, a sample of which is shown in Fig. 1. We consider a group of CUEs, $\mathcal{M} = \{CUE^m | m = 1, ..., M\}$, that communicate with one BS in a traditional cellular mode. We assume that the CUEs use M orthogonal channels for the transmission without any interference among themselves [2]. There is a group of IoTDs, $\mathcal{K} = \{IoTD^k | k = 1, ..., K\}$, that communicate with one IoT GW directly via D2D communication, where all nodes are equipped with a single antenna. It is assumed that the CUEs are uniformly distributed in the cell while IoTDs are uniformly distributed within a disc of radius r_{max} around the GW. We assume that $h_{c,b}$, $h_{c,g}$, $h_{i,b}$ and $h_{i,g}$ represent the gains of the channels CUE-to-BS, CUE-to-GW, IoTD-to-BS and IoTD-to-GW, respectively.

We assume that all the channels follow the conventional path loss model accompanied with small scale Rayleigh fading, namely $PL_o^{1/2}\, d_{\eta,\mu}^{-\alpha/2} h_{\eta,\mu}$, where $d_{\eta,\mu}$ is the distance between node η and node μ, α is the path-loss exponent, PL_o is the path-loss constant and $h_{\eta,\mu} \sim \mathcal{CN}(0,1)$. We also assume that the BS knows the locations of the users within the cell, and hence perfect CSI is available at the BS whose responsibility is to pair each CUE and each IoTD and determine their transmit power.

[2]The orthogonality among the M CUE channels can be achieved in different systems by separating them in time, frequency or code domain

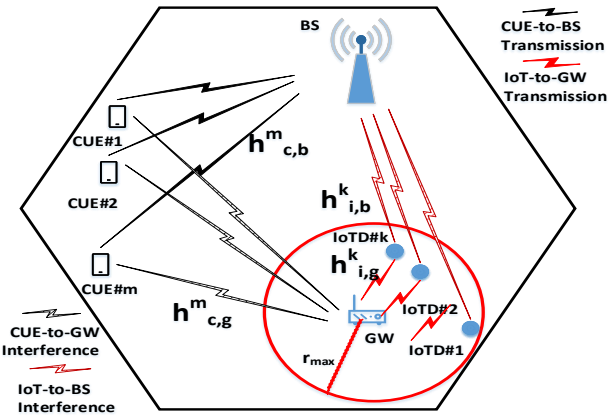

Fig. 1: A sample scenario that a cluster of K IoTDs reuse the resources of M cellular users (CUE) to communicate with a central IoT gateway (GW) node for the uplink transmission.

The signals received at the BS and the GW due to the transmissions of both the CUE and the IoTD are given in (1), respectively.

$$y_b = \sqrt{P_c^m}\, h_{c,b}\, S_c^m + \sqrt{P_d^k}\, h_{i,b}\, S_d^k + n_b, \tag{1a}$$

$$y_g = \sqrt{P_c^m}\, h_{c,g}\, S_c^m + \sqrt{P_d^k}\, h_{i,g}\, S_d^k + n_g, \tag{1b}$$

where S_c^m denotes the information symbol transmitted from the m^{th} CUE to the BS, and S_d^k denotes the information symbol transmitted from the k^{th} IoTD to the GW, with the information that $E\{|S_c^m|^2\} = 1$ and $E\{|S_d^k|^2\} = 1$, respectively. n_b and n_g are the complex additive white Gaussian noises (AWGN) at the BS and the GW, respectively with a distribution $\mathcal{CN}(0, N_o)$. P_c^m and P_d^k are the transmit power level of the CUE and the IoTD, respectively. The corresponding SINR at the BS and the GW are given by

$$\gamma_{c,b}^m = \frac{P_c^m\, \lambda_{x_1}\, x_1}{P_d^k\, \lambda_{y_1}\, y_1 + N_o}, \tag{2a}$$

$$\gamma_{i,g}^k = \frac{P_d^k\, \lambda_{y_2}\, y_2}{P_c^m\, \lambda_{x_2}\, x_2 + N_o}, \tag{2b}$$

where N_o is the AWGN noise power, $x_1 = |h_{c,b}|^2, x_2 = |h_{c,g}|^2, y_1 = |h_{i,b}|^2$ and $y_2 = |h_{i,g}|^2$ are the fading gain of the channels which follow exponential distribution with unit mean, and $\lambda_t = PL_o d_t^{-\alpha}$ for subscript $t \in \{x_1, x_2, y_1, y_2\}$. We assume that both the destinations have certain QoS constraints that need to be satisfied in order to correctly decode the received signals from the CUE and the IoTD. In other words, the m^{th} CUE is a candidate partner of the k^{th} IoTD if and only if the QoS interference constraints ($\gamma_{c,b}^m \geq \Gamma_C$) and ($\gamma_{i,g}^k \geq \Gamma_I$) are satisfied, where Γ_C and Γ_I are the threshold SINR values at the BS and the GW, respectively.

III. Interference Management Schemes

In this section, given that one IoTD and one CUE share a single RB for the transmission, we briefly describe two interference management schemes that help achieve their predefined QoS requirements.

A. Fixed Power Margin (FPM) Scheme

Referring to the FPM scheme in [9], a minimum SINR (Γ_C) is required by the CUE to maintain the QoS requirement at the BS. Let us assume that there is at most Υ proportion of the threshold SINR allowed in order to control the introduced interference from the IoTD to the CUE. If the IoTD controls its introduced interference perfectly, the CUE achieves the required QoS (i.e., Γ_C) by scaling its own transmit power, P_c^m, by a factor of Υ. In other words, in the absence of interference from the IoTD, the CUE link achieves $\Upsilon\,\Gamma_C$ signal-to-interference (SIR or SINR with zero interference) as follows.

$$\frac{P_c^m\,\lambda_{x_1}\,x_1}{N_o} \geq \Upsilon\,\Gamma_C. \tag{3}$$

The existence of Υ factor introduces a bound on the CUE transmit power which can be found by re-arranging the relation in (3) as follows.

$$P_c^m \geq \frac{P_c^{eNB}}{x_1\,\lambda_{x_1}}, \tag{4}$$

where ($P_c^{eNB} = \Upsilon\,\Gamma_C\,N_o$) represents the received power at the BS from the CUE. Knowing the value of this power margin, the BS is able to determine whether the IoTD is able to achieve its own QoS requirement by controlling the transmit power (P_d^k) while avoiding harmful interference to the CUE. Referring to the interference-limited derivations in [5] and assuming that the m^{th} CUE uses the lower bound of P_c^m as in (4), the following SIR condition must be satisfied.

$$\frac{P_c^{eNB}}{P_d^k\,\lambda_{y_1}\,y_1} \geq \Gamma_C, \tag{5}$$

which represents the CUE SIR assuming N_o is negligible with respect to the IoTD interference. Therefore, the upper bound of the transmit power of any IoTD that reuses the same uplink RB of the m^{th} CUE is given by

$$P_d^k \leq \frac{P_c^{eNB}}{\Gamma_C\,y_1\,\lambda_{y_1}}. \tag{6}$$

Assuming a prefect knowledge of the channel gain, the bound in (4) provides the transmit power of the CUE such that the OP becomes zero. However, if N_o is not negligible with respect to the interference term, the CUE's OP will not be accurate if the upper bound in (6) is used. To solve this, the upper bound of P_d^k needs to be re-defined for the exact scheme which can be derived from (5) without neglecting N_o as follows.

$$\begin{aligned} P_d^k &\leq \frac{P_c^{eNB} - \Gamma_C\,N_o}{\Gamma_C\,y_1\,\lambda_{y_1}}, \\ &\leq \frac{(\Upsilon-1)\,N_o}{y_1\,\lambda_{y_1}}. \end{aligned} \tag{7}$$

Since the maximum IoTD transmit power is limited by the node power (P_d^{max}), the transmit power that maximizes the IoTD achievable throughput can be decidedin terms of the distance between the IoTD and the BS (i.e., d_{y_1}), which is given for the interference-limited case and the exact case in (8a) and (8b), respectively.

$$P_d^k = \begin{cases} \frac{P_c^{eNB}}{\Gamma_C\,y_1\,\lambda_{y_1}}, & d_{y_1} \leq D_{m1} \\ P_d^{max}, & \text{otherwise}, \end{cases} \tag{8a}$$

$$P_d^k = \begin{cases} \frac{(\Upsilon-1)\,N_o}{y_1\,\lambda_{y_1}}, & d_{y_1} \leq D_{m2}, \\ P_d^{max}, & \text{otherwise}. \end{cases} \tag{8b}$$

where D_{m1} and D_{m2} are given by

$$D_{m1} = \left(\frac{P_d^{max}\,PLo\,y_1}{\Upsilon\,N_o}\right)^{\frac{1}{\alpha}},\ D_{m2} = \left(\frac{P_d^{max}\,PLo\,y_1}{(\Upsilon-1)\,N_o}\right)^{\frac{1}{\alpha}}. \tag{9}$$

In this scheme, the IoTD is allowed to transmit using its maximum power as long as it is far from the BS. However, if the IoTD is close to the BS within the threshold distance (i.e., D_{m1} and D_{m2}) defined in (9), the IoTD must limit its transmit power.

In order to avoid the need of instantaneous CSI feedback for the IoTD-CUE pair association and the power allocation in (8), it is possible to compare d_{y1} with the mean value of D_{mi} which is a function of exponentially distributed fading value y_1. The same approach is adopted in [9] for the power allocation based on the statistical estimation of the fading value in the absence of coordination and feedback facilities between the IoTD-CUE pair. The estimation of D_{mi} is given as follows.

$$\begin{aligned} E[D_{mi}] &= \epsilon_i\,E[y^{\frac{1}{\alpha}}], \\ &= \epsilon_i\,\textstyle\int_0^\infty y^{\frac{1}{\alpha}} e^{-y_1} dy_1, \\ &= \epsilon_i\,\Gamma(1+\tfrac{1}{\alpha}). \end{aligned} \tag{10}$$

where $\epsilon_1 = \left(\frac{P_d^{max}\,PLo}{\Upsilon\,N_o}\right)^{\frac{1}{\alpha}}$, $\epsilon_2 = \left(\frac{P_d^{max}\,PLo}{(\Upsilon-1)\,N_o}\right)^{\frac{1}{\alpha}}$, and $\Gamma(.)$ is the Gamma function defined in (8.310) [18]. For the sake of simplicity in the analysis, we consider the perfect CSI case to bound the performance of the system.

B. Cooperative Pairing (CooP) Scheme

In contrast to the FPM scheme, the CooP scheme is such that both nodes cooperate and adjust their transmit power to achieve the QoS requirements at the two destinations. Similar to us, the CUE-D2D cooperation has already been investigated in [11], however to maximize the overall network throughput.

IV. Derivation of Outage Probability

In order to find whether an arbitrary IoTD can access the network, we need to find the OP for that IoTD, which shares one of the M RBs with one of the M active CUEs. Since the CUE OP over the orthogonal RBs are independent, we can express the total OP over multiple RBs, P_{out}^{MC}, as follows.

$$P_{out}^{MC} = \prod_{m=1}^{M} P_{out}^m, \tag{11}$$

where P_{out}^m represents the joint OP of pairing the k^{th} IoTD with the m^{th} CUE given that the their deployment locations are known (i.e., conditional probability for a given deployment scenario). In other words, P_{out}^m can be defined as the probability that either the corresponding IoTD cannot satisfy the QoS

requirement at the GW or the CUE cannot satisfy its QoS requirement at the BS, which can be expressed as follows.

$$P_{out}^{m} = \Pr\{\gamma_{c,b}^{m} \leq \Gamma_C \text{ or } \gamma_{i,g}^{k} \leq \Gamma_I\}. \tag{12}$$

In the following, we manipulate the derivations of the OPs for the two interference management schemes.

A. Outage Probability under the Interference-Limited FPM Scheme

In this sub-section, we derive the OP for the FPM scheme under the interference-limited scenario. Taking the power control in (4) and (8a) into account, the two SINRs $(\gamma_{c,b}^{m}, \gamma_{i,g}^{k})$ in (2) can be expressed as follows.

$$\gamma_{c,b}^{m} = \begin{cases} \Gamma_C, & d_{y_1} \leq D_{m1}, \\ \frac{P_c^{eNB}}{P_d^{max}\, y_1\, \lambda_{y_1}}, & \text{otherwise}, \end{cases} \tag{13a}$$

$$\gamma_{i,g}^{k} = \begin{cases} \frac{x_1\, y_2\, \lambda}{x_2\, y_1\, \Gamma_C}, & d_{y_1} \leq D_{m1}, \\ \frac{x_1\, y_2\, P_d^{max}\, \lambda_L}{x_2\, P_c^{eNB}}, & \text{otherwise}. \end{cases} \tag{13b}$$

where $\lambda = \frac{\lambda_{y_2}\lambda_{x_1}}{\lambda_{y_1}\lambda_{x_2}}$ and $\lambda_L = \frac{\lambda_{y_2}\lambda_{x_1}}{\lambda_{x_2}}$. Substituting the two SINRs in (13) into (12), the OP under the interference-limited FPM scheme can be expressed as follows.

$$P_{out}^{FPMI} = \begin{cases} Pr\{Z \leq \mu\} & , d_{y_1} \leq D_{m1} \\ Pr\{\frac{1}{y_1} \leq v \text{ or } L \leq \Gamma_L\} & , \text{otherwise} \end{cases} \tag{14}$$

where FPMI stands for the interference-limited case. Z, Γ_{th}, v, L, and Γ_L are given by

$$Z = \frac{Z_2}{Z_1} = \frac{x_1\, y_2}{x_2\, y_1}, \mu = \Gamma_{th}\lambda,\ \Gamma_{th} = \Gamma_C\, \Gamma_I, \tag{15a}$$

$$L = \frac{x_1\, y_2}{x_2} = \frac{Z_2}{x_2}, v = \frac{P_d^{max}\, \lambda_{y_1}}{\Upsilon\, N_o}, \Gamma_L = \frac{\Upsilon\, \Gamma_{th}\, N_o}{P_d^{max}\, \lambda_L}. \tag{15b}$$

Notice that the first branch in (14) consists of one probability term (i.e., $Pr\{Z \leq \mu\}$), while the second branch consists of two terms (i.e., $Pr\{\Theta_1 \text{ or } \Theta_2\} = Pr\{\frac{1}{y_1} \leq v \text{ or } L \leq \Gamma_L\}$). The reason is that the QoS of the CUE for $(d_{y_1} \leq D_{m1})$ is satisfied as $\gamma_{c,b}^{m} = \Gamma_C$ holds in (13b) which means that the OP of the CUE is zero.

In order to derive the OP for each of the interference management schemes in closed form, the probability density function (PDF) of the product and the ratio of two random variables (RVs) need to be evaluated. We employ the Mellin transform (MT) technique [19]–[22] to assist us deriving a closed-form expression for the PDF of the product and the ratio of two independent exponentially distributed RVs [19]. The MT technique is used in the literature to derive the PDF of the product of Rayleigh distributed RVs in [20] and Nakagami-m distributed RVs in [22]. The MT is one of the family of integral transform techniques, similar to the Fourier and Laplace transform techniques. *Theorem* 1 provides a closed-form expression of the OP under the interference-limited FPM scheme by evaluating the probabilities in (14) for exponential RVs.

Theorem 1: *The OP under the interference-limited FPM scheme is given as follows.*

$$P_{out}^{FPMI} = \begin{cases} 1 - \frac{1-\mu(1-\ln(\mu))}{(-1+\mu)^2} & , d_{y_1} \leq D_{m1}, \\ \exp(-1/v)\,(1 - Pr\{\Theta_2\}) & \\ \quad + Pr\{\Theta_2\} & , \text{otherwise}. \end{cases} \tag{16}$$

where $Pr\{\Theta_2\}$ is given by

$$Pr\{\Theta_2\} = \Gamma_L\, G_{2\,2}^{2\,2}\left(\begin{smallmatrix}\{-1,0\},\{-\} \\ \{0,0\},\{-1\}\end{smallmatrix} \middle| \Gamma_L\right). \tag{17}$$

where $G_{p\ q}^{m\ n}\left(\begin{smallmatrix}a_1,\ldots,a_p \\ b_1,\ldots,b_q\end{smallmatrix} \middle| z\right)$ is the hyper-geometric MeijerG function [17], [18].

Proof: Refer to *Appendix A*.

B. Outage Probability under the Exact FPM Scheme

In this sub-section, we derive the OP under the FPM scheme considering the exact evaluation of the SINR (i.e., N_o is not negligible). Taking the power control in (4) and (8b) into account, the two SINRs $(\gamma_{c,b}^{m}, \gamma_{i,g}^{k})$ in (2) can be expressed as follows.

$$\gamma_{c,b}^{m} = \begin{cases} \Gamma_C & , d_{y_1} \leq D_{m2}, \\ \frac{\Upsilon\, \Gamma_C\, N_o}{P_d^{max}\, \lambda_{y_1}\, y_1 + N_o} & , \text{otherwise}, \end{cases} \tag{18a}$$

$$\gamma_{i,g}^{k} = \begin{cases} \frac{(\Upsilon-1) x_1\, y_2\, \lambda_L}{y_1\,(\lambda_{x_1}\, x_1 + \Upsilon\, \Gamma_C\, \lambda_{x_2}\, x_2)} & , d_{y_1} \leq D_{m2}, \\ \frac{x_1\, y_2\, P_d^{max}\, \lambda_{x_1}\, \lambda_{y_2}}{(\lambda_{x_1}\, x_1 + \Upsilon\, \Gamma_C\, \lambda_{x_2}\, x_2)\, N_o} & , \text{otherwise}. \end{cases} \tag{18b}$$

Substituting the two SINRs in (18) into (12), the OP under the exact FPM scheme can be expressed as follows.

$$P_{out}^{FPME} = \begin{cases} Pr\{Z_e \leq A_{th}\} & , d_{y_1} \leq D_{m2}, \\ Pr\{\frac{1}{y_1 + \beta} \leq C_{th} \text{ or } Z_g \leq B_{th}\} & , \text{otherwise}, \end{cases} \tag{19}$$

where FPME stands for the exact FPM case, and the other parameters and RVs are given as follows.

$$Z_e = \frac{Z_2}{Z_w},\ Z_g = \frac{Z_2}{x_w},\ Z_w = y_1\, x_w, \tag{20a}$$

$$x_w = x_1 + w\, x_2,\ w = \frac{\Upsilon\, \Gamma_C\, \lambda_{x_2}}{\lambda_{y_1}}, \beta = \frac{N_o}{P_d^{max} \lambda_{y_1}}, \tag{20b}$$

$$A_{th} = \frac{\Gamma_I}{(\Upsilon - 1)\ \lambda}, B_{th} = \frac{\Gamma_I\, N_o}{P_d^{max}\, \lambda_L}, C_{th} = \frac{1}{\Upsilon\, N_o\, P_d^{max}\, \lambda_{y_1}}. \tag{20c}$$

Theorem 2 provides a closed-form expression of the OP under the exact FPM scheme by evaluating the probabilities in (19) for exponential RVs.

Theorem 2: *The OP under the exact FPM scheme is given as follows.*

$$P_{out}^{FPME} = \begin{cases} 1 - \frac{G_{11} - G_{12}}{Ath\,(1-w)} & , d_{y_1} \leq D_{m2}, \\ G_2\ (1 - \exp(-H_1)) & \\ \quad + \exp(-H_1) & , \text{otherwise}. \end{cases} \tag{21}$$

where the parameters are given by

$$G_{11} = G_{3\,3}^{2\,3}\left(\begin{matrix}\{-1,-1,0\},\{\}\\ \{0,0\},\{-1\}\end{matrix}\middle|\frac{1}{A_{th}}\right), \tag{22a}$$

$$G_{12} = G_{3\,3}^{2\,3}\left(\begin{matrix}\{-1,-1,0\},\{\}\\ \{0,0\},\{-1\}\end{matrix}\middle|\frac{1}{w\,A_{th}}\right), \tag{22b}$$

$$G_2 = \frac{1}{1-w}\left(G_{21} - G_{22}\right), \tag{22c}$$

$$G_{21} = B_{th}\, G_{2\,3}^{2\,2}\left(\begin{matrix}\{-1,0\},\{\}\\ \{0,0\},\{-1\}\end{matrix}\middle|B_{th}\right), \tag{22d}$$

$$G_{22} = w\, B_{th}\, G_{2\,3}^{2\,2}\left(\begin{matrix}\{-1,0\},\{\}\\ \{0,0\},\{-1\}\end{matrix}\middle|w\, B_{th}\right), \tag{22e}$$

$$H_1 = \frac{1}{C_{th}} - \beta. \tag{22f}$$

Proof: Refer to *Appendix B*.

C. Outage Probability under the CooP Scheme

Given the SINRs in (2), *Theorem 3* provides a closed-form expression of an arbitrary IoTD-CUE pair under the CooP scheme.

Theorem 3: *The CUE-IoTD OP under the CooP scheme is given as follows.*

$$P_{out}^{C} = 1 - \psi_c\,\phi_i \exp\left(-N_o\left(\frac{\Gamma_C}{P_c^m\,\lambda_{x_1}} + \frac{\Gamma_I}{P_d^k\,\lambda_{y_2}}\right)\right). \tag{23}$$

where ψ_c and ϕ_i are given by

$$\psi_c = \frac{P_c^m \lambda_{x_1}}{P_c^m \lambda_{x_1} + P_d^k \lambda_{y_1}\,\Gamma_C}, \tag{24a}$$

$$\phi_i = 1 - \frac{P_d^k\,\lambda_{y_2}}{P_d^k\,\lambda_{y_2} + P_c^m \lambda_{x_2}\,\Gamma_I}. \tag{24b}$$

Proof: Refer to *Appendix C*.

D. Outage-Optimal Power Allocation for the CooP Scheme

In the previous sub-sections, there is no need to optimize power allocation in the FPM scheme as it is already set in the design of the scheme in equations (4) and (8). While in the CooP scheme we need to search for the optimal values of the two powers. However, the aforementioned derivations for the CooP scheme are not based on the optimal power allocation. Other literature such as [11] considers the power allocation for this case targeting on the maximization of system throughput. Consequently, here, we study a CooP-based optimal power allocation scheme from the prospective of OP (i.e., minimizing the OP) to provide a fair comparison between both the candidate interference management schemes. The proposed optimization problem is formulated as follows.

$$P_1: \quad \min_{P_c^m, P_d^k} \quad P_{out} = 1 - \frac{f\left(P_c^m, P_d^k\right)}{g\left(P_c^m, P_d^k\right)} \tag{25a}$$

$$\text{s.t.} \quad 0 < P_c^m < P_c^{max} \tag{25b}$$

$$0 < P_d^k < P_d^{max}, \tag{25c}$$

where f and g can be found from (23) and (24), respectively, which are given by

$$f(P_c^m, P_d^k) = P_c^m P_d^k \lambda_{y_1}\lambda_{x_2}, \tag{26a}$$

$$g(P_c^m, P_d^k) = \left(a\,(P_c^m)^2 + b\,(P_d^k)^2 + c\,P_c^m P_d^k\right), \times \exp\left(N_o\left(\frac{\Gamma_C}{P_c^m\,\lambda_{x_1}} + \frac{\Gamma_I}{P_d^k\,\lambda_{y_2}}\right)\right), \tag{26b}$$

$$a = \lambda_{x_1}\lambda_{x_2}\Gamma_I,\ b = \lambda_{y_1}\lambda_{y_2}\Gamma_C, \tag{26c}$$

$$c = \lambda_{x_1}\lambda_{y_2} + \Gamma_C\Gamma_I\lambda_{y_1}\lambda_{x_2}. \tag{26d}$$

P_1 can be re-casted to the following equivalent form.

$$P_2: \quad \max_{P_c^m, P_d^k} \quad \frac{f(P_c^m, P_d^k)}{g(P_c^m, P_d^k)} \tag{27a}$$

$$\text{s.t.} \ 0 < P_c^m < P_c^{max} \tag{27b}$$

$$0 < P_d^k < P_d^{max} \tag{27c}$$

The optimization problem in (27) takes the similar form of a concave fractional programming problem [23], which is represented in the literature as

$$H(x) = \tfrac{f(x)}{g(x)}, \tag{28}$$

over the set $S = \{x \in C, h_k(x) \leq 0, k = 1, ..., m\}$. This type of problem can be solved via several different techniques. First, it can be indirectly solved by the concave programming methods via variable transformation as in [24]. Second, the Dinkelbach algorithm has been used in the literature for solving the concave fractional and nonlinear fractional programming problems [23], [25], [26], via which the optimal solution can be found by solving a set of non-linear convex sub-problems in an iterative manner. The sample of such a non-linear convex sub-problem is defined by parameter ($q \in R$) as follows.

$$\pi(q) = \max\{\, f(x) \,-\, q\, g(x) : x \in S\}. \tag{29}$$

An optimal solution to the problem in (29) can be found using classical methods such as the Bisection and the Newton-Raphson methods [27] which satisfies $q^* = H^*$. However, the Dinkelbach algorithm cannot be adopted directly to solve the problem in (27) since both $f(P_c^m, P_d^k)$ and $g(P_c^m, P_d^k)$ are not jointly concave and convex, respectively, in terms of P_c^m and P_d^k, respectively. It can be easily proved that $f(g)$ is concave (convex) with respect to one of the two optimization variables when the other one is fixed. Knowing this, we propose an iterative alternating Dinkelbach (IAD) algorithm to find the optimal solution for the outage-optimal power allocation in the CooP scheme. The detailed steps of the IAD algorithm are summarized in *Algorithm 1*.

The IAD algorithm proposed herein aims at minimizing the OP of the CooP scheme by alternatively optimizing the transmit power of the IoTD and the CUE based on two iterative Dinkelbach sub-algorithms. In the first Dinkelbach sub-algorithm, the transmit power of the IoTD is iteratively optimized assuming a fixed initial value of the CUE transmit power (P_d^{max}). The output of the first sub-algorithm (i.e., $(P_d^k)^{(1)}$) is fed as input to the second Dinkelbach sub-algorithm that iteratively optimizes the CUE transmit power to $(P_c^m)^{(1)}$ assuming the input IoTD transmit power is fixed at $(P_d^k)^{(1)}$. Aforementioned two steps jointly is one complete

Algorithm 1: The proposed iterative alternating Dinkelbach (IAD) algorithm.

1 **Initialization:** Set an initial value for the CUE power: $(P_c^m)^{(0)} = P_d^{max}$, the objective value $P_{out}(0) = 1$, the convergence parameter $\epsilon = 1e-5$ and the iteration index $u = 1$.
2 **While** no convergence ($\Delta P_{out} \geq \epsilon$), **do**
3 Apply the standard iterative Dinkelbach algorithm to find the optimal IoTD power $(P_d^k)^{(u)}$ that minimizes the IoTD OP for a fixed $P_c^m = (P_c^m)^{(u-1)}$.
4 Apply the standard iterative Dinkelbach algorithm to find the optimal CUE power $(P_c^m)^{(u)}$ that minimizes the CUE OP for a fixed $P_d^k = (P_d^k)^{(u)}$.
5 Calculate $P_{out}(u)$ using $(P_c^m)^{(u)}$ and $(P_d^k)^{(u)}$ using (25a).
6 Calculate $\Delta P_{out} = |P_{out}(u) - P_{out}(u-1)|$.
7 $u = u + 1$
8 **End While**
9 **Output:** $(P_c^m)^{(*)}$ and $(P_d^k)^{(*)}$

iteration of the IAD algorithm. In the second iteration of the algorithm, instead of using P_d^{max} as initial value for the CUE transmit power, we adopt the optimal value of the first iteration (i.e., $(P_c^m)^{(1)}$) as the initial point and repeat the same steps until the objective value is converged or maximum number of iterations (u_{max}) is reached as shown in *Algorithm 1*.

For a sample system, Fig. 2 shows the convergence event of the outage-optimum CooP scheme using the proposed IAD algorithm while comparing with the iterative quadratic transform method in [28]. As per the intermediate step of the proposed IAD algorithm, the bisection and the Newton-Raphson methods are adopted to solve the problem in (29). In the figure, we show the tagged CUE-IoTD OP with the increasing iterations. It is clear from the figure that the IAD algorithm with Newton-Raphson method has the fastest convergence rate compared to that with the bisection method and the quadratic transform method, which coincides with the results in [27] and [28], respectively. The work in [27] reported a higher convergence rate of the Newton-Raphson method compared to the bisection method. On the other hand, the iterative quadratic transform method [28], which was proposed to solve the single and multiple-ratio concave-convex problems, exhibits a lower convergence rate for the single-ratio problems compared to the Dinkelbach algorithm.

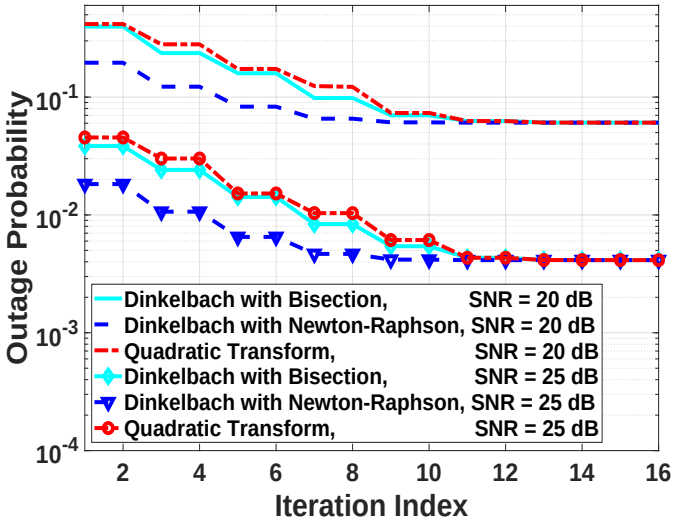

Fig. 2: A sample convergence proof of the IAD algorithm using both the Newton-Raphson and bisection methods compared to the iterative quadratic transform method for 20 and 25 dB SNR.

V. Performance Evaluation

In this section, we verify the correctness of the derived OP for two interference management schemes via simulation. Moreover, we provide various useful insights in deploying IoTDs in a conventional cellular network. For this purpose, we conduct an extensive simulation, the parameters of which are as follows. The number of deployed CUEs and IoTDs are 30 and 20, respectively, where the CUEs are uniformly deployed within the cell of radius 1000 m and the IoTDs are uniformly deployed within a cluster of radius $r_{max} = 30$ m unless mentioned otherwise. Moreover, the path-loss exponent α is set to 4, and the path-loss constant is 0.1. In the following, each data point for the OP is the average of $1e+4$ iterations while considering the average of 30×20 possible deployed pairs in each iteration.

Fig. 3 shows the average pair OP with the increasing value of SNR. Two deployment scenarios are investigated in this figure, where different values of the distance between the GW and the BS are considered (i.e., 300 m and 800 m) for a QoS requirement ($\Gamma_I = \Gamma_C = -5$ dB). The value of the power margin for the exact FPM scheme (Υ) is 3 dB. For each deployment scenario, the exact FPM scheme and three CooP schemes (low interference regime "LIR", high interference regime "HIR" and outage-optimal power allocation) are com-

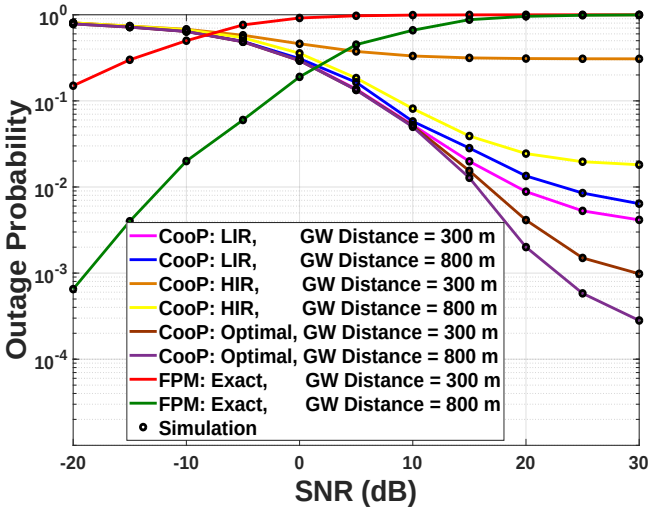

Fig. 3: The average pair OP with the increasing SNR, where ($\Gamma_I = \Gamma_C = -5$ dB) and ($\Upsilon = 3$ dB) for two GW distances (300 and 800 m).

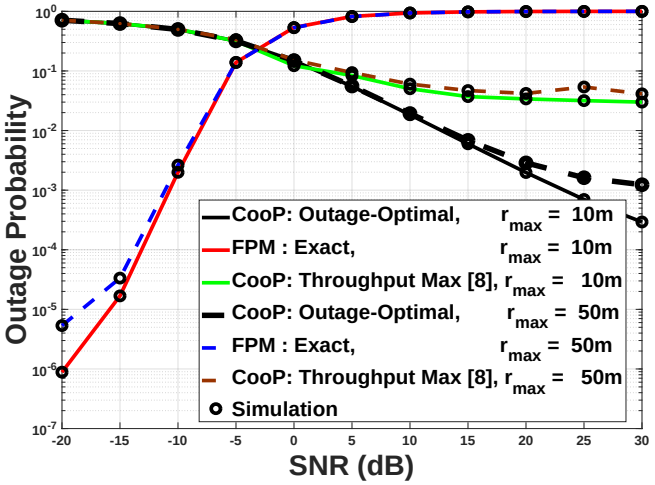

Fig. 4: The pair OP with the increasing SNR, where ($\Gamma_I = \Gamma_C = -5$ dB), $\Upsilon = 3$ dB and GW distance = 500 m for two IoT cluster radius ($r_{max} = 10$ and 50) m.

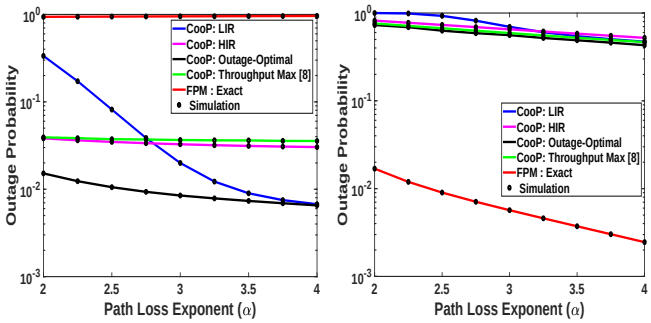

(a) (b)

Fig. 6: The pair OP with the increasing value of pass-loss exponent (α) for two SNR values $\rho = 20$ and -5 dB.

pared. The comparison of the three CooP schemes is provided to show the effect of using an optimal power allocation on the CooP interference management scheme. The interference ratio (I_r) of the CooP scheme, defined as the ratio of the power allocated to the IoTD and that allocated to the CUE, can be expressed as

$$I_r = 10 \log_{10} \left(\frac{P_d^k}{P_c^m} \right), \tag{30}$$

where the values of I_r in Fig. 3 are -40 dB and -10 dB for the LIR and HIR, respectively. The optimal output of the IAD algorithm is used for the outage-optimal CooP scheme.

Fig. 3 reveals an interesting finding about the FPM and CooP schemes with the increasing transmit SNR. The results show that the OP resultant from the CooP scheme improves as the SNR increases in contrast to the FPM scheme, the resultant OP of which becomes worse due to the fixed power margin that must be maintained to protect the CUE. This means that it becomes harder for the FPM scheme to find a suitable partner of the tagged IoTD when the SNR is high. This figure further shows that the OP achieved by all schemes improves as the distance between the BS and the GW increases. This is justified as the average interference level of the CUEs imposed by the IoTDs is decreasing with the increasing distance. Moreover, the accuracy of the analytical results under different interference management schemes is verified through numerical simulations in this figure.

For the CooP scheme, Fig. 3 also shows that the HIR with the 800 m deployment scenario leads to a worse OP compared to the LIR with the 300 m deployment one, which reveals the importance of developing an optimal power allocation scheme. In both the deployment scenarios, the outage-optimal power allocation scheme outperforms the other two schemes.

In Fig. 4, we investigate the effect of IoT cluster radius on the OP under the outage-optimal CooP scheme, the throughput-optimal CooP scheme in [11], and the exact FPM scheme. In this figure, the QoS requirement ($\Gamma_I = \Gamma_C$) is -5 dB, Υ is 3 dB and the GW distance is 500 m. The figure shows that the OP improves as the IoT cluster radius decreases from 50 to 10 m. This is due to the fact that the interference sources are limited to a smaller area around the cluster head (i.e., the GW) when we have a smaller cluster radius. The results further reveal that the proposed outage-optimal scheme incurs better OP compared to the throughput-optimal scheme in [11].

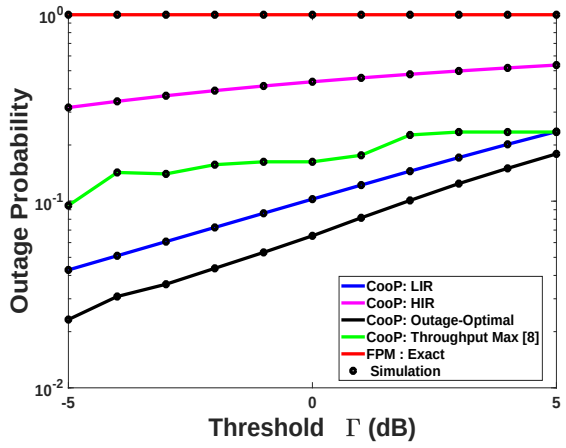

Fig. 5: The pair OP with the increasing threshold ($\Gamma = \Gamma_I = \Gamma_C$) for $\Upsilon = 3$ dB, SNR = 15 dB and GW distance = 300 m.

Fig. 5 shows the average pair OP with respect to the QoS threshold ($\Gamma = \Gamma_C = \Gamma_I$) under a fixed power margin $\Upsilon = 3$ dB and transmit SNR = 15 dB for a GW at a distance of 300 m. The results confirm the intuition that the average OP incurred by all schemes increase with the increasing QoS requirement of the two nodes. The proposed outage-optimal CooP scheme incurs the best OP compared to all the other schemes.

Fig. 6 shows the average pair OP resulting from the proposed outage-optimal CooP scheme with respect to the path-loss exponent (α) under two SNR values (i.e., 20 dB and -5 dB). In this figure, the OP decreases under all the schemes when α increases. This behavior is due to the assumption about the path-loss model in which the channel gain is inversely proportional to α that results in less interference level to the nodes. Consequently, increasing α decreases the OP of the

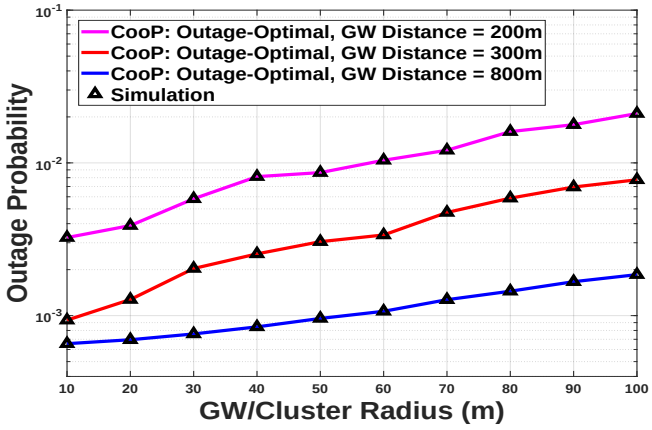

Fig. 7: The pair OP of the proposed outage-optimal CooP scheme with the increasing IoT cluster radius (r_{max}) , where $\Gamma_I = \Gamma_C = -10$ dB and SNR = 20 dB for three GW distances (200, 300 and 800 m).

IoTD-CUE pair which coincides with the improvement of the success probability (i.e., 1-OP) with the increasing α in [29]. The results reveals that the decreasing rate of the OP under the LIR CooP scheme is higher compared to the other schemes due to the inherent low-interference in this scheme.

Fig. 7 shows the OP resulting from the proposed outage-optimal CooP scheme with respect to the IoT cluster radius (r_{max}) under the settings with $\Gamma_I = \Gamma_C = -10$ dB and SNR = 20 dB. The results confirm the observation in Fig. 4 about the improved OP when r_{max} decreases. However, in this figure, we investigate the OP for three deployment scenarios with the IoT cluster at 200, 300 and 800 m distance from the BS. We can notice different changing rate of the OP between the near and far deployment scenarios. The increasing rate of OP (with the increasing r_{max}) for the near deployment scenario is larger compared to the far deployment scenario. This is due to the fact that increasing radius for a near deployment scenario implies that IoT devices are more likely located near the BS compared to a far deployment scenario.

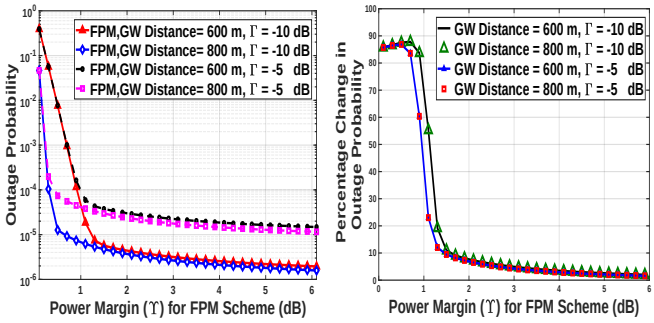

(a) (b)

Fig. 8: The OP and the percentage change in the OP resultant from the FPM scheme with the increasing power margin (i.e., Υ) under the two cell deployment scenarios (the GW is 600 m and 800 m away from the cell center location) and for -5 and -10 dB QoS requirements ($\Gamma = \Gamma_C = \Gamma_I$).

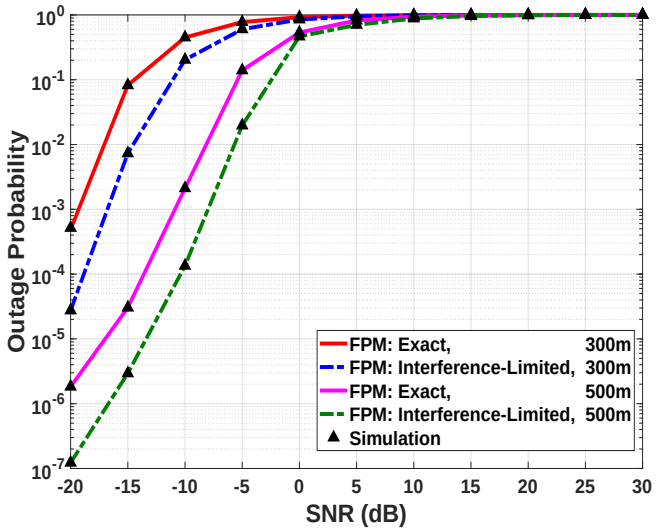

Fig. 9: Comparison of the OP between the exact FPM scheme and the interference-limited FPM scheme with respect to the increasing SNR under two cell deployment scenarios (the GW is located 300 and 500 m away from the cell center location).

Fig. 8a shows the average pair OP incurred by the FPM scheme with respect to the increasing power margin (i.e., Υ) for two cell deployment scenarios (the GW is located at 600 m and 800 m away from the cell center) under -5 dB and -10 dB QoS requirements ($\Gamma = \Gamma_C = \Gamma_I$). The results show a high improvement in the OP when Υ increases from its initial small value 0.1 dB up to 1 dB. The rate of improvement decreases from 1 to 3 dB and diminishes afterwards. These results are more strengthened in Fig. 8b where the average OP reduces from 90% to 10% when Υ changes from 0 to 1 dB, and from 10% to around 4% when Υ changes from 1 to 3 dB. Fig. 8a also shows that the average OP depends on both the QoS requirement (Γ) and the distance between the GW and the BS. However, we notice that the saturated value of OP is more dependent on Γ.

Fig. 9 compares the resulting average OP between the interference-limited FPM and the exact FPM schemes. The analytical and simulation results show that both the schemes achieve almost the same OP when the transmit SNRs are as high as -5 or 0 dB, where the PSD of the AWGN (i.e., N_o) is negligible with respect to the IoTD interference. However, for the lower SNR values, N_o cannot be neglected as it is comparable to the interference term. Since the FPM scheme is outage-optimum in the low SNR regime, this justifies the importance of the analytically derived OP under the exact FPM scheme while taking the spectrum reuse constraint into account.

VI. Conclusion

In this work, in order to enable the deployment of clustered IoTDs under cellular networks, we investigated D2D communication as an effective technology that improves the spectral efficiency greatly. While taking the QoS requirements of the CUEs into full consideration, two interference management schemes were investigated from the perspective of OP. The

OP of an arbitrary CUE-IoTD pair under the exact FPM, interference-limited FPM and CooP schemes were analytically derived in closed form expression. Theoretical and simulation results revealed that the CooP scheme is the outage-optimal one in the high SNR regime while the FPM scheme is the optimal one for the low SNR regime. The results further showed that the optimal range of the fixed power margin parameter (Υ) under the FPM scheme lies in between 2 and 3 dB. As of future work, we plan to investigate the performance of an underlaid D2D system assuming that multiple IoTDs share the same spectrum band of each CUE.

Appendix A
Interference-limited FPM Scheme: Outage Probability Derivation

- **Case 1:** ($d_{y_1} \leq D_{m1}$)

The PDF of an exponentially distributed RV X with q mean is given by

$$f_X(x) = q \exp(-q\,x) \tag{31}$$

The MT, $M_X(s)$, of the same exponentially distributed RV is given by

$$M_X(s) = q^{1-s}\,\Gamma(s), \tag{32}$$

where $\Gamma(s)$ is the Gamma function. In order to find the OP for this case, we need to find the PDF of Z, $f_Z(z)$, which is expressed as the ratio of two RVs, i.e., Z_1 and Z_2, in (15), where both are product of two exponentially distributed RVs with unit-mean. With the help of (2.2) in [21], the MT of Z_1 and Z_2 can be evaluated as the product of MTs of the corresponding RVs, we refer it as the product rule, which is given as follows.

$$M_{Z_1}(s) = M_{x_2}(s)\,M_{y_1}(s) = \Gamma^2(s), \tag{33a}$$
$$M_{Z_2}(s) = M_{x_1}(s)\,M_{y_2}(s) = \Gamma^2(s). \tag{33b}$$

With the help of (2.3) in [21], the MT on the ratio of two RVs, Z_1 and Z_2, (we refer it as the ratio rule) is given by

$$\begin{aligned} M_Z(s) &= M_{Z_2}(s)\,M_{Z_1}(2-s), \\ &= \Gamma^2(s)\,\Gamma^2(2-s), \end{aligned} \tag{34}$$

The PDF of Z can be found using the inverse MT technique, which is given by

$$f_Z(z) = \frac{2 - 2\,z + (1+z)\ln(z)}{(-1+z)^3}. \tag{35}$$

Finally, the OP for the first case can be evaluated as follows.

$$\begin{aligned} P_{out}^{I_1} &= Pr\{Z \leq \mu\} = 1 - \int_{\mu}^{\infty} f_Z(z)\,\mathrm{d}z, \\ &= 1 - \frac{1 - \mu\,(1 - \ln(\mu)\,)}{(-1+\mu)^2}. \end{aligned} \tag{36}$$

The result of this integration concludes the first case in (16).

- **Case 2:** ($d_{y_1} > D_{m1}$)

The OP for the second case in (14) is defined as the probability of occurring of one event or another, $Pr\{\Theta_1 \text{ or } \Theta_2\}$, where $Pr\{\Theta_1\} = Pr\{\frac{1}{y_1} \leq v\}$ and $Pr\{\Theta_2\} = Pr\{L \leq \Gamma_L\}$ which are derived as follows.

☐ Probability of Θ_1:

One possible method to obtain the probability of Θ_1 is using reciprocal distribution formula [30] for continuous RVs where the PDF of the RV $y_x = \frac{1}{y_1}$ is given as follows.

$$f_{y_x}(y_x) = \frac{1}{y_1^2} f_{y_1}(\frac{1}{y_1}). \tag{37}$$

Then, by replacing (y_1) in the PDF of the exponential RV y_1 with $1/y_1$, the probability of Θ_1 can be evaluated as follows.

$$\begin{aligned} Pr\{\Theta_1\} &= 1 - \int_{v}^{\infty} f_{y_x}(y_x)\,\mathrm{d}y_x, \\ &= \exp\left(-1/v\right). \end{aligned} \tag{38}$$

☐ Probability of Θ_2:

With the help of (6-59) in [31], the PDF of L could be derived in terms of joint PDF of the variables Z_2 and x_2, i.e., $f_{Z_2 x_2}(Z_2, x_2)$, as follows.

$$\begin{aligned} f_L(L) &= \int_0^{\infty} x_2\, f_{Z_2 x_2}(x_2\,L, x_2)\,\mathrm{d}x_2, \\ &\overset{(a)}{=} \int_0^{\infty} x_2\, f_{Z_2}(x_2\,L) f_{x_2}(x_2)\,\mathrm{d}x_2. \end{aligned} \tag{39}$$

where (a) is due to the independence between Z_2 and x_2, and the PDF of Z_2, $f_{Z_2}(Z_2)$, can be found using the inverse MT technique in (33b) which is given as follows.

$$f_{Z_2}(Z_2) = 2\,K_0(2\,\sqrt{Z_2}) \tag{40}$$

where $K_n(.)$ is the modified Bessel function of the second kind. Given that $x_2 \sim Exp(1)$ with a PDF $f_{x_2}(x_2) = e^{-x_2}$, the integration in (39) can be expressed as

$$\begin{aligned} f_L(L) &= 2 \int_0^{\infty} x_2 \exp(-x_2) K_0(2\,\sqrt{L}\sqrt{x_2})\,\mathrm{d}x_2, \\ &\overset{(b)}{=} \int_0^{\infty} x_2\, G_{0\,1}^{1\,0}\left(\begin{matrix}\{-\},\{-\}\\ \{0\},\{-\}\end{matrix}\middle| x_2\right) \\ &\quad \times G_{0\,2}^{2\,0}\left(\begin{matrix}\{-\},\{-\}\\ \{0,0\},\{-\}\end{matrix}\middle| L\,x_2\right)\,\mathrm{d}x_2. \end{aligned} \tag{41}$$

where (b) follows from converting both the exponential and the Bessel functions into equivalent hyper-geometric MeijerG functions using (11) and (14) in [32], respectively. Using (21) and (22) in [32], the integration in (41) can be found which is given as follows.

$$f_L(L) = G_{1\,2}^{2\,1}\left(\begin{matrix}\{-1\},\{-\}\\ \{0,0\},\{-\}\end{matrix}\middle| L\right). \tag{42}$$

With the help of (26) in [32], the probability of Θ_2, which represents the OP of the IoTD, can be evaluated as follows.

$$\begin{aligned} Pr\{\Theta_2\} &= \int_0^{\Gamma_L} f_L(L)\,\mathrm{d}L, \\ &= \Gamma_L\, G_{2\,3}^{2\,2}\left(\begin{matrix}\{-1,0\},\{-\}\\ \{0,0\},\{-1\}\end{matrix}\middle| \Gamma_L\right), \end{aligned} \tag{43}$$

where Γ_L is given in (15). Knowing that Θ_1 and Θ_2 are independent events, the OP of the the second case in (14) can be then evaluated using (38) and (43) as

$$\begin{aligned} P_{out}^{I_2} &= Pr\{\Theta_1\, or\, \Theta_2\}, \\ &= Pr\{\Theta_1\} + Pr\{\Theta_2\} - Pr\{\Theta_1\}\,Pr\{\Theta_2\}, \\ &= \exp\left(-1/v\right)\,(1 - Pr\{\Theta_2\}) + Pr\{\Theta_2\}. \end{aligned} \tag{44}$$

which concludes the proof.

APPENDIX B
EXACT FPM SCHEME: OUTAGE PROBABILITY DERIVATION

- **Case 1:** $(d_{y_1} \leq D_{m2})$

In order to find the PDF and CDF of Z_e, we have to find the PDF of both x_w and Z_w in addition to the PDF of Z_2 given in (40).

△ **Derivation for $f_{x_w}(x_w)$ and $f_{Z_w}(Z_w)$:**

Assume that $x_w = x_1 + \tilde{x_2}$, where $\tilde{x_2} = w\, x_2$. With the help of (5-18) in [31], the PDF of $\tilde{x_2}$ is given by

$$f_{\tilde{x_2}}(\tilde{x_2}) = \tfrac{1}{w} \exp\left(\tfrac{-x_2}{w}\right). \tag{45}$$

Knowing the PDF of both x_1 and $\tilde{x_2}$ and with the help of (6-44) in [31], the PDF of x_w can be found as follows.

$$\begin{aligned} f_{x_w}(x_w) &= \int_0^{x_w} f_{x_1}(x_1) f_{\tilde{x_2}}(x_w - x_1)\, \mathrm{d}x_1, \\ &= \frac{1}{1-w}\left(e^{(-x_w)} - e^{\left(\frac{-x_w}{w}\right)}\right), \end{aligned} \tag{46}$$

By applying the MT to (45) and (46) and using the product rule, we can find the MT for the PDF of Z_w which is given as follows.

$$\begin{aligned} M_{Z_w}(s) &= M_{y_1}(s)\, M_{x_w}(s), \\ &= \Gamma(s)\, \tfrac{1}{1-w}\left(\Gamma(s) - (\tfrac{1}{w})^{-s}\, \Gamma(s)\right). \end{aligned} \tag{47}$$

With the help of inverse MT, the PDF of Z_w is given as follows.

$$f_{Z_w}(Z_w) = \tfrac{2}{1-w}\left(K_0\left(a_w\sqrt{Z_w}\right) - K_0\left(b_w\sqrt{Z_w}\right)\right), \tag{48}$$

where $a_w = 2$, and $b_w = \frac{2}{\sqrt{w}}$. With the help of (6-59) in [31] and similar to the PDF of L in (39), the PDF of Z_e could be derived using the joint PDF of both Z_2 and Z_w, which is given as follows.

$$\begin{aligned} f_{Z_e}(Z_e) &= \int_0^{\infty} Z_w\, f_{Z_2 Z_w}(Z_w\, Z_e, Z_w)\, \mathrm{d}Z_w, \\ &= \tfrac{4}{1-w}\,(I_1 - I_2), \end{aligned} \tag{49}$$

where the I_1 and I_2 are defined as follows.

$$I_1 = \int_0^{\infty} Z_w K_0\left(\tilde{a_2}\sqrt{Z_w}\right) K_0\left(a_w\sqrt{Z_w}\right) \mathrm{d}Z_w, \tag{50a}$$

$$I_2 = \int_0^{\infty} Z_w K_0\left(\tilde{a_2}\sqrt{Z_w}\right) K_0\left(b_w\sqrt{Z_w}\right) \mathrm{d}Z_w. \tag{50b}$$

where $\tilde{a_2} = 2\sqrt{Z_e}$.

△ **Derivation of the integrals I_1 and I_2:**

Using (14) in [32], the two Bessel functions can be expressed as equivalent hyper-geometric MeijerG functions and hence I_1 can be re-casted as follows.

$$\begin{aligned} I_1 = \int_0^{\infty} \frac{Z_w}{4} G_{0\,2}^{2\,0}\left(\begin{matrix}\{-\},\{-\}\\ \{0,0\},\{-\}\end{matrix}\middle| Z_e\, Z_w\right) \\ \times G_{0\,2}^{2\,0}\left(\begin{matrix}\{-\},\{-\}\\ \{0,0\},\{-\}\end{matrix}\middle| Z_w\right) \mathrm{d}Z_w. \end{aligned} \tag{51}$$

Using (21) and (22) in [32], I_1 is given as follows.

$$I_1 = \frac{Z_e^{-2}}{4} G_{2\,2}^{2\,2}\left(\begin{matrix}\{-1,-1\},\{-\}\\ \{0,0\},\{-\}\end{matrix}\middle| \frac{1}{Z_e}\right). \tag{52}$$

Using the same derivations of I_2, we obtain

$$I_2 = \frac{Z_e^{-2}}{4} G_{2\,2}^{2\,2}\left(\begin{matrix}\{-1,-1\},\{-\}\\ \{0,0\},\{-\}\end{matrix}\middle| \frac{1}{w\, Z_e}\right). \tag{53}$$

Using (52), (53) and (49), the CDF of Z_e, which represent the OP of the first case in (19), is given as follows.

$$\begin{aligned} F_{Z_e}(A_{th}) &= 1 - \int_{A_{th}}^{\infty} f_{Z_e}(Z_e)\, dZ_e, \\ &= 1 - \frac{1}{1-w}\,(I_3 - I_4), \end{aligned} \tag{54}$$

where the integrations I_3 and I_4 are defined as follows.

$$I_3 = \int_{A_{th}}^{\infty} Z_e^{-2} G_{2\,2}^{2\,2}\left(\begin{matrix}\{-1,-1\},\{-\}\\ \{0,0\},\{-\}\end{matrix}\middle| \frac{1}{Z_e}\right) \mathrm{d}Z_e, \tag{55a}$$

$$I_4 = \int_{A_{th}}^{\infty} Z_e^{-2} G_{2\,2}^{2\,2}\left(\begin{matrix}\{-1,-1\},\{-\}\\ \{0,0\},\{-\}\end{matrix}\middle| \frac{1}{w\, Z_e}\right) \mathrm{d}Z_e. \tag{55b}$$

Both integration can be solved through a variable transformation, $x = Z_e^{-1}$, followed by integration of the MeijerG function using (26) in [32] which is given as follows.

$$\begin{aligned} I_3 &= \frac{1}{A_{th}} G_{3\,3}^{2\,3}\left(\begin{matrix}\{-1,-1,0\},\{-\}\\ \{0,0\},\{-1\}\end{matrix}\middle| \frac{1}{A_{th}}\right), \\ I_4 &= \frac{1}{A_{th}} G_{3\,3}^{2\,3}\left(\begin{matrix}\{-1,-1,0\},\{-\}\\ \{0,0\},\{-1\}\end{matrix}\middle| \frac{1}{w\, A_{th}}\right). \end{aligned} \tag{56}$$

It is now possible to substitute the relation in (56) into (54) to obtain the final value of the first case in (21). This concludes the proof of *Case 1* under the exact FPM scheme.

- **Case 2:** $(d_{y_1} \geq D_{m2})$

The OP for the second case in (19) is defined as the probability of occurring of one event or another, $Pr\{\Omega_1 \,\mathrm{or}\, \Omega_2\}$, where $Pr\{\Omega_1\} = Pr\{\frac{1}{y_1+\beta} \leq C_{th}\}$ and $Pr\{\Omega_2\} = Pr\{Z_g \leq B_{th}\}$ which are derived as follows.

□ Probability of Ω_1:

One possible method to obtain the probability of Ω_1 is as follows.

$$\begin{aligned} Pr\{\Omega_1\} &= Pr\{\frac{1}{y_1+\beta} \leq C_{th}\} = Pr\{y_1 > \frac{1 - C_{th}\,\beta}{C_{th}}\}, \\ &= \exp\left(-H_1\right). \end{aligned} \tag{57}$$

where $H_1 = \frac{1}{C_{th}} - \beta$.

□ Probability of Ω_2:

One possible method to obtain $Pr\{\Omega_2\} = Pr\{Z_g \leq B_{th}\}$ is to adopt the same approach used to obtain the probability of Θ_2 via the joint PDF of x_w and Z_2. With the help of (6-59) in [31], (40) and (46), the PDF of Z_g is derived as follows.

$$\begin{aligned} f_{Z_g}(Z_g) &= \int_0^{\infty} x_w\, f_{Z_2 x_w}(x_w\, Z_g, x_w)\, \mathrm{d}x_w, \\ &= \int_0^{\infty} x_w\, f_{Z_2}(x_w\, Z_g)\, f_{x_w}(x_w)\, \mathrm{d}x_w, \\ &= \frac{2}{1-w}\,(I_5 - I_6). \end{aligned} \tag{58}$$

where the integrations I_5 and I_6 are given as follows.

$$I_5 = \int_0^{\infty} x_w \exp\left(-x_w\right) K_0\left(a_2\sqrt{x_w}\right) \mathrm{d}x_w, \tag{59a}$$

$$I_6 = \int_0^{\infty} x_w \exp\left(\frac{-x_w}{w}\right) K_0\left(a_2\sqrt{x_w}\right) \mathrm{d}x_w. \tag{59b}$$

Using (11) and (14) in [32] followed by (21) and (22) in [32], I_5 and I_6 can be evaluated as follows.

$$I_5 = \frac{1}{2} G_{1\,2}^{2\,1}\left(\begin{matrix}\{-1\},\{-\}\\ \{0,0\},\{-\}\end{matrix}\middle| Z_g\right), \tag{60a}$$

$$I_6 = \frac{w}{2} G_{1\,2}^{2\,1}\left(\begin{matrix}\{-1\},\{-\}\\ \{0,0\},\{-\}\end{matrix}\middle| w\, Z_g\right). \tag{60b}$$

Using (58) and (60), the CDF of Z_g is given as follows.

$$\begin{aligned} F_{Z_g}(B_{th}) = Pr\{\Omega_2\} &= \int_0^{B_{th}} f_{Z_g}(Z_g)\, dZ_g, \\ &= \frac{1}{1-w}\left(I_7 - w\, I_8\right), \end{aligned} \tag{61}$$

where

$$I_7 = \int_0^{B_{th}} G_{1\,2}^{2\,1}\left(\begin{matrix}\{-1\},\{-\}\\ \{0,0\},\{-\}\end{matrix}\middle| Z_g\right) \mathrm{d}Z_g, \tag{62a}$$

$$I_8 = \int_0^{B_{th}} G_{1\,2}^{2\,1}\left(\begin{matrix}\{-1\},\{-\}\\ \{0,0\},\{-\}\end{matrix}\middle| w\, Z_g\right) \mathrm{d}Z_g. \tag{62b}$$

With the help of (26) in [32], I_7 and I_8 can be solved as follows.

$$I_7 = B_{th}\, G_{2\,3}^{2\,2}\left(\begin{matrix}\{-1,0\},\{-\}\\ \{0,0\},\{-1\}\end{matrix}\middle| B_{th}\right), \tag{63a}$$

$$I_8 = B_{th}\, G_{2\,3}^{2\,2}\left(\begin{matrix}\{-1,0\},\{-\}\\ \{0,0\},\{-1\}\end{matrix}\middle| w\, B_{th}\right), \tag{63b}$$

It is now possible to substitute the relation in (63) into (61) to find the probability of Ω_2 as follows.

$$F_{Z_g}(B_{th}) = Pr\{\Omega_2\} = \frac{1}{1-w}\left(G_{21} - G_{22}\right), \tag{64}$$

where G_{21} and G_{22} are given in (22). The OP of the second case under the exact FPM scheme can be found in the similar way as in (44), which is given in (21). This concludes the proof of *Theorem 2*.

Appendix C
Outage Probability Derivation: CooP Scheme

In order to the find the OP under the CooP scheme, we derive the OP of the CUE and the IoTD individually in the following.

☐ CooP Scheme: The CUE OP

The OP of the CUE, i.e., $Pr(\gamma_{c,b}^m \leq \Gamma_C)$, under the CooP scheme is derived by re-arranging the relation in (2a) as follows.

$$\gamma_{c,b}^m = \frac{\alpha_1\, x_1}{y_1 + \beta_1} = \frac{x_{11}}{y_{11}}, \tag{65}$$

where $\alpha_1 = \frac{P_c^m\, \lambda_{x_1}}{P_d^k\, \lambda_{y_1}}$ and $\beta_1 = \frac{N_o}{P_d^k\, \lambda_{y_1}}$. With the help of (5-18) in [31], the PDF of x_{11} and y_{11} are expressed as follows.

$$f_{x_{11}}(x_{11}) = \frac{1}{\alpha_1} \exp\left(\frac{-x_1}{\alpha_1}\right) U(x_1), \tag{66a}$$

$$f_{y_{11}}(y_{11}) = \exp\left(-\left(y_1 - \beta_1\right)\right) U(y_1 - \beta_1), \tag{66b}$$

where x_1 and y_1 are exponentially distributed RVs, and $U(.)$ is the unit-step function. The PDF of the RV $z_m = x_{11}/y_{11}$ cab be evaluated using (6-59) in [31] as follows.

$$\begin{aligned} f_{z_m}(z_m) &= \int_{\beta_1}^{\infty} y_{11}\, f_{x_{11}y_{11}}(y_{11} z_m, y_{11}) dy_{11}, \\ &= \left(\frac{\beta_1}{\alpha_1 + z_m} + \frac{\alpha_1}{(\alpha_1 + z_m)^2}\right) \exp(\frac{-z_m\, \beta_1}{\alpha_1}). \end{aligned} \tag{67}$$

Using the integration by parts, the CDF of z_m is given by

$$\begin{aligned} F_{z_m}(z_m) &= \int_0^{z_m} f_{z_m}(z_m)\, dz_m, \\ &= 1 - \frac{\alpha_1}{\alpha_1 + z_m} \exp\left(\frac{-z_m\, \beta_1}{\alpha_1}\right). \end{aligned} \tag{68}$$

The OP of the CUE can be found by substituting α_1, β_1 and $z_m = \Gamma_C$ to get $F_{z_m}(\Gamma_C)$, which is as follows.

$$Pr\{\gamma_{c,b}^m \leq \Gamma_C\} = 1 - \psi_c \exp\left(\frac{-N_o\, \Gamma_C}{P_c^m\, \lambda_{x_1}}\right), \tag{69}$$

where ψ_c is given in (24a).

☐ CooP Scheme: The IoTD OP

The OP of the IoTD under the CooP scheme is derived by re-arranging the relation in (2b) as follows.

$$\gamma_{i,g}^k = \frac{\alpha_2\, y_2}{x_2 + \beta_2} = \frac{y_{22}}{x_{22}}, \tag{70}$$

where $\alpha_2 = \frac{P_d^k\, \lambda_{y_2}}{P_c^m\, \lambda_{x_2}}$ and $\beta_2 = \frac{N_o}{P_c^m\, \lambda_{x_2}}$. With the help of (5-18) in [31], the PDF of y_{22} and x_{22} are expressed as follows.

$$f_{y_{22}}(y_{22}) = \frac{1}{\alpha_2} \exp\left(\frac{-y_2}{\alpha_2}\right) U(y_2), \tag{71a}$$

$$f_{x_{22}}(x_{22}) = \exp\left(-(x_2 - \beta_2)\right) U(x_2 - \beta_2), \tag{71b}$$

where x_2 and y_2 are exponentially distributed random variables. Using the same technique as in (67), the CDF of the RV ($z_i = y_{22}/x_{22}$) can be expressed as follows.

$$F_{z_i}(z_i) = 1 - \frac{\alpha_2}{\alpha_2 + z_i} \exp\left(\frac{-z_i\, \beta_2}{\alpha_2}\right). \tag{72}$$

The OP of the IoTD, $Pr\{\gamma_{i,g}^k \leq \Gamma_I\}$, can be found by substituting α_2, β_2 and $z_i = \Gamma_I$ to obtain $F_{z_i}(\Gamma_I)$, which represents the OP of the IoTD as follows.

$$Pr\{\gamma_{i,g}^k \leq \Gamma_I\} = 1 - \phi_i \exp\left(\frac{-N_o\, \Gamma_I}{P_d^k\, \lambda_{y_2}}\right), \tag{73}$$

where ϕ_i is given in (24b).

☐ CooP Scheme: The CUE-IoTD OP

Using the similar steps in (44), the OP of the arbitrary CUE-IoTD pair is given in (23) which concludes the proof of *Theorem 3*.

References

[1] S. H. Shah and I. Yaqoob, "A survey: Internet of things (IoT) technologies, applications and challenges," in *Proc. IEEE SEGE*, Aug 2016, pp. 381–385.

[2] "IEEE standard for air interface for broadband wireless access systems," *IEEE Std 802.16-2012 (Revision of IEEE Std 802.16-2009)*, pp. 1–2542, Aug 2012.

[3] Z. Chen, Z. Ding, X. Dai, and R. Zhang, "An optimization perspective of the superiority of NOMA compared to conventional OMA," *IEEE Trans. Signal Process*, vol. 65, no. 19, pp. 5191–5202, Oct 2017.

[4] J. Liu, N. Kato, J. Ma, and N. Kadowaki, "Device-to-device communication in LTE-advanced networks: a survey," *IEEE Commun. Surveys Tuts.*, vol. 17, no. 4, pp. 1923–1940, 2015.

[5] M. M. Elmesalawy, "D2D communications for enabling Internet of things underlaying LTE cellular networks," *Journal of Wireless Networking and Communications*, vol. 6, no. 1, pp. 1–9, 2016.

[6] L. Liu and W. Yu, "A D2D-based protocol for ultra-reliable wireless communications for industrial automation," *IEEE Trans. on Wire. Communic.*, pp. 1–1, May 2018, Early Access.

[7] O. Bello and S. Zeadally, "Intelligent device-to-device communication in the internet of things," *IEEE Syst. J.*, vol. 10, no. 3, pp. 1172–1182, Sept 2016.

[8] Y. Li, K. Chi, H. Chen, Z. Wang, and Y. h. Zhu, "Narrowband internet of things systems with opportunistic D2D communication," *IEEE Internet Things J.*, pp. 1–1, Dec. 2017.

[9] B. Kaufman, J. Lilleberg, and B. Aazhang, "Spectrum sharing scheme between cellular users and ad-hoc device-to-device users," *IEEE Trans. Wireless Commun.*, vol. 12, no. 3, pp. 1038–1049, Mar 2013.

[10] B. Kaufman and B. Aazhang, "Cellular networks with an overlaid device to device network," in *Proc. Asilomar Conference on Signals, Systems and Computers*, Oct 2008, pp. 1537–1541.

[11] D. Feng, L. Lu, Y. Yuan-Wu, G. Y. Li, G. Feng, and S. Li, "Device-to-device communications underlaying cellular networks," *IEEE Trans. Commun*, vol. 61, no. 8, pp. 3541–3551, Aug 2013.

[12] K. M. S. Huq, S. Mumtaz, and J. Rodriguez, "Outage probability analysis for device-to-device system," in *Proc. IEEE ICC*, May 2016, pp. 1–5.

[13] S. Joshi and R. K. Mallik, "Coverage and interference in D2D networks with Poisson cluster process," *IEEE Commun. Lett.*, vol. 22, no. 5, pp. 1098–1101, May 2018.

[14] J. Sun, T. Zhang, X. Liang, Z. Zhang, and Y. Chen, "Uplink resource allocation in interference limited area for D2D-based underlaying cellular networks," in *Proc. IEEE VTC Spring*, May 2016, pp. 1–6.

[15] S. Joshi and R. K. Mallik, "Analysis of dedicated and shared device-to-device communication in cellular networks over Nakagami-m fading channels," *IET Communications*, vol. 11, no. 10, pp. 1600–1609, 2017.

[16] J. Park and J. H. Lee, "Semi-distributed spectrum access to enhance throughput for underlay device-to-device communications," *IEEE Trans. Commun.*, vol. 65, no. 10, pp. 4572–4582, Oct 2017.

[17] R. Beals and J. Szmigielski, "Meijer G–functions: A gentle introduction," *Notes of The American Mathematical Society*, vol. 60, no. 7, pp. 866–872, Aug 2013.

[18] I. M. Ryzhik and I. S. Gradshteyn, *Table of integrals, series, and products*, 7th ed., A. Jeffrey and D. Zwillinger, Eds. Academic Press, 2007.

[19] J. Galambos and I. Simonelli, *Products of random variables: applications to problems of physics and to arithmetical functions*. Marcel Dekker, Inc., 2004.

[20] J. Salo, H. M. El-Sallabi, and P. Vainikainen, "The distribution of the product of independent Rayleigh random variables," *IEEE Trans. Antennas Propag.*, vol. 54, no. 2, pp. 639–643, Feb 2006.

[21] R. D. Prasad, "Probability distributions of algebraic functions of independent random variables," *SIAM Journal on Applied Mathematics*, vol. 18, no. 3, pp. 614–626, 1970.

[22] S. Ahmed, L. L. Yang, and L. Hanzo, "Probability distributions of products of Rayleigh and Nakagami-m variables using mellin transform," in *Proc. IEEE ICC*, Jun 2011, pp. 1–5.

[23] W. Dinkelbach, "On nonlinear fractional programming," *Management Science*, vol. 13, no. 7, pp. 492–498, 1967.

[24] P. Pardalos and A.T.Pillips, "Global optimization of fractional programs," *Journal of Global Optimization*, vol. 1, pp. 173–182, 1991.

[25] R. G. Ródenas, M. L. López, and D. Verastegui, "Extensions of Dinkelbach's algorithm for solving non-linear fractional programming problems," *Top*, vol. 7, no. 1, pp. 33–70, Jun 1999.

[26] B. Bossy, P. Kryszkiewicz, and H. Bogucka, "Optimization of energy efficiency in the downlink LTE transmission," in *Proc. IEEE ICC*, May 2017, pp. 1–6.

[27] T. Ibaraki, "Parametric approaches to fractional programs," *Mathematical Programming*, vol. 26, no. 3, pp. 345–362, Oct 1983.

[28] K. Shen and W. Yu, "Fractional programming for communication systems-Part I: Power control and beamforming," *IEEE Trans. Signal Process.*, vol. 66, no. 10, pp. 2616–2630, May 2018.

[29] U. Schilcher, S. Toumpis, M. Haenggi, A. Crismani, G. Brandner, and C. Bettstetter, "Interference functionals in poisson networks," *IEEE Trans. Inf. Theory*, vol. 62, no. 1, pp. 370–383, Jan 2016.

[30] M. Escobar and J. Moreno-Jiménez, "Reciprocal distributions in the analytic hierarchy process," *European Journal of Operational Research*, vol. 123, no. 1, pp. 154 – 174, 2000.

[31] A. Papoulis and S. U. Pillai, *Probability, random variables and stochastic processes*, 4th ed. McGraw-Hill, 2002.

[32] V. Adamchik and O. I. Marichev, "The algorithm for calculating integrals of hypergeometric type functions and its realization in reduce system," in *Proc. International Symposium on Symbolic and Algebraic Computation,ACM, Academic Press*, 1990, pp. 212–224.